JOURNAL OF MATERIALS SCIENCE **35** (2000) 2573–2579

Mechanism of localized corrosion of aluminum–silicon carbide composites in a chloride containing environment

Z. AHMAD
King Fahd University of Petroleum & Minerals, KFUPM Box # 1748, Dhahran-31261, Saudi Arabia
E-mail: ahmadz@kfupm.edu.sa

P. T. PAULETTE
Naval Research Laboratory, Washington D.C 20375-5343, USA
E-mail: paulette@anvil.anvil.nrl.navy.mil

B. J. A. ALEEM
King Fahd University of Petroleum & Minerals, KFUPM Box # 590, Dhahran-31261, Saudi Arabia
E-mail: abaleem@kfupm.edu.sa

In marine environments, more pits develop on SiC reinforced aluminum alloy composites than on their unreinforced counterparts. Although it has been suggested that the SiC plays an active role in composite corrosion by fostering the initiation of pits, this fact has not been conclusively demonstrated. The present paper considers data of two independent investigations concerning the effects of alloy type, and heat treatment on pit initiation in SiC reinforced aluminum composites. For four alloys, it is shown that pit initiation is dependent on the alloy type and heat treatment. Further, microscopic observations show that pit initiation sites are correlated with secondary phase particles. Results suggest that secondary phases, rather than the SiC particles, contribute to the pitting behavior of the composites.

1. Introduction

Because of the evolution of applications with demanding performance criteria in recent years, attention has shifted considerably from conventional to newly emerging engineering materials. Materials development is now focused on high performance polymers, advanced ceramics, and composites for a wide variety of applications. Aluminum alloy 6013 is an Al-Mg-Si-Cu alloy developed in recent years by Alcoa. It has a 15% higher tensile strength than alloy 6061-T6 and a good resistance to corrosion [1, 2]. Because of the combination of attractive mechanical properties, weldability, formability and corrosion resistance, alloy 6013 is finding increasing applications in aerospace, defense, automotive and general structural applications [3, 4]. The development of Al 6013 reinforced with 20 vol % SiC is a recent occurance [5, 6]. The composite exhibits a higher fracture toughness and mechanical strength than its unreinforced counterpart. Similar behaviour has been observed for Al 2024, Al 5456 and Al 6061 [7, 8]. The corrosion behavior of Al 6013-20 SiC has been recently described [9]. Pitting is the major form of localized attack on Al 6013-20 SiC in chloride solutions. A larger number of pits are formed on the composite than on Al 6013, however, they are shallower and more widely spread. The presence of secondary phases such as Mg_2Si makes the SiC rich areas, SiC-matrix interface or secondary phases highly reactive, however, there is no clear evidence to show whether the pits nucleate on SiC rich areas, SiC matrix interface or at secondary phases. Identification of the pit initiation sites is vital to an understanding of pitting mechanism in metal matrix composites. In this work, experimental results of corrosion investigations on Al 6013-20 SiC are compared with similar results from other aluminum alloys, in order to contribute to the enhancement of knowledge on the corrosion mechanism of Al-SiC composites in chloride environment.

1.1. Experimental

Silicon Carbide was blended with Al 6013 aluminium powder. The mixture was consolidated in a billet 18 inches diameter. The billet was extruded to a 3 inches diameter rod. The rods were forged and rolled to a 0.1 inch thick steel. The sheets were then left in the as fabricated condition or heat treated to O or T4 temper. T4 was heated at 546° C for an hour and aged for one day.

TABLE I Nominal compositions of the aluminum alloys

Alloy designation	Heat treatment	Si	Fe	Cu	Mn	Mg	Cr	Zn	Ti	Al
6013	T-4, 0	0.6	0.5	1.0	0.8	0.8	0.1	0.25	0.1	Balance
6061	T-6	0.6	—	0.27	1.0	1.0	0.2	—	—	Balance
5456	T-6	—	—	—	0.8	5.1	0.12	—	—	Balance
2024	T-6	4.4	—	—	0.6	1.5	—	—		Balance

The grain size of the composites was 10 microns obtained at 500×. The distribution and size of the silicon carbide particulate, SiC(P) is observed best at 100×, 500× and 1000×. The nominal compositions of the aluminum alloys considered in this work are given in Table I. All alloys listed above except 5456 are heat treatable.

1.1.1. Sample preparation

The samples were successively ground with 320, 400 and 600 grit SiC and polished with 6 micron diamond paste on struers Dac cloth and rinsed in de-mineralized H_2O and ethyl alcohol, followed by struer 0.04 μm silica op Nap. These samples were given one of the three heat treatments. (1) Solution treatment at 325°C for 30 minutes followed by aging at room temperature, (T4). (2) Annealing at 350°C for three hours followed by furance cooling, (O). (3) Samples as fabricated (F). All other alloys had a T6 heat treatment and were ground to 600 grit prior to electro-chemical polarization.

1.1.2. Test media

All tests for Al 6013 were conducted in 3.5 wt% NaCl. Tests for all other alloys were conducted in 0.1 N NaCl (de-aerated).

1.1.3. Exposure tests for pitting

Experiments were conducted in triplicates in accordance with ASTM Standard G-31-72. Samples after preparation were exposed in 3.5 wt% NaCl for 1000 hours under open air contact. The solution was gently stirred. The samples which were exposed to 3.5% NaCl were treated with a mixture of 20 g potassium dichromate ($K_2Cr_rO_7$) and 28 ml (28 cm^{-1}) orthophosphoric acid in distilled water. Disc specimens of 1.5 cm diameter were used.

1.1.4. Electrochemical measurements

Potentiodynamic cyclic pitting scanning technique was used to obtain pitting potential of metal matrix composites mentioned in Table I. Cyclic potentiodynamic polarization measurement technique has been applied to determine the susceptibility of Al 6013-20SiC(P) to pitting. A detailed standard procedure for carrying out the above test is laid down in ASTM standard G61 [10]. The specimen is anodically polarized starting from corrosion potential (E_{corr}) until the current density reaches a predetermined value ($6.5 \times 10^{-3} \mu A/cm^2$) when the scan is reversed and the alloy is polarized in the cathodic direction until the forward and reverse scan intersect. Two important parameters, pitting potential (E_p) and protection potential (E_{pp}) are obtained from the curve. A typical cyclic polarization curve is shown in Fig. 1.

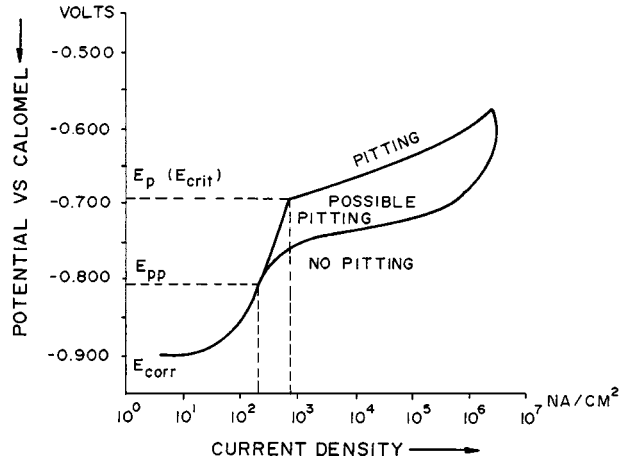

Figure 1 A typical cyclic polarization curve.

1.1.5. Microanalytical studies

All microanalytical studies were conducted by a low vacuum scanning electron microscope (LV SEM). In LVSEM, an additional pumping system has been added so that the specimen chamber can be maintained in low vacuum while the column is in a high vacuum state. This will void the problem of charging a specimen with complicated surface morphology. A microanalysis system with a Quant Map software package for X-ray mapping was used for Energy Dispersive Spectroscopy (EDS) studies.

X-ray diffraction (XRD) studies were conducted on a 6013-20 SiC sample. Diffraction pattern was generated by a theta −2 theta diffractometer. The angled scan was 4 to 80° 2 θ.

2. Results and discussions

Electrochemical polarization data for the alloys and composites is shown in Table II where E_p is the pitting potential and ΔE is the difference between the steady state (E_{corr}) and pitting potential E_p. From this table it can be seen that the pitting potential of the monolithic materials depends upon the alloy composition and is always more positive (less active and less pitting prone) than that of the reinforced material [7, 8]. Of the composites materials, the pitting resistance follows the order, Al 2024 = Al 6013-20SiC(P) F > Al

TABLE II Pitting data for alloys and composites

Materials designation	Potential (mV) mV vs S.C.E	Av. pitting depth (μm)	$\Delta E = E_p - E_{corr}$ mV vs S.C.E
Al 6013-20 SiC(P)-T4	−690 [Ref. 9]	10	443
Al 6013-20 SiC(P)-F	−640 [Ref. 9]	47.33	360
Al 6013-20 SiC(P)-O	−650 [Ref. 9]	27.66	350
Al 2024	−680 [Ref. 8]	—	525
Al 5456	−690 [Ref. 8]	—	411
Al 6061	−640 [Ref. 8]	—	632
SiC/Al 2024	−640 [Ref. 8]	—	259
SiC/Al 6061	−665 [Ref. 8]	—	443

6013-20SiC(P)-0 > Al 6061 > Al 6013 20SiC(P)-T4 = Al 5456. These test results show that the pitting resistance of these materials is dependent on three factors, the alloy, the heat treatment and the presence of the reinforcement (SiC).

The pitting data of alloys 6013, 2024, 6061 and composites is given in Table II. Pitting was the major form of localized corrosion on all three tempers of alloy 6013-20SiC and other composites (Table II). Pits were predominantly hemispherical and elliptical in shape (Fig. 2). Crystallographic pitting was also observed.

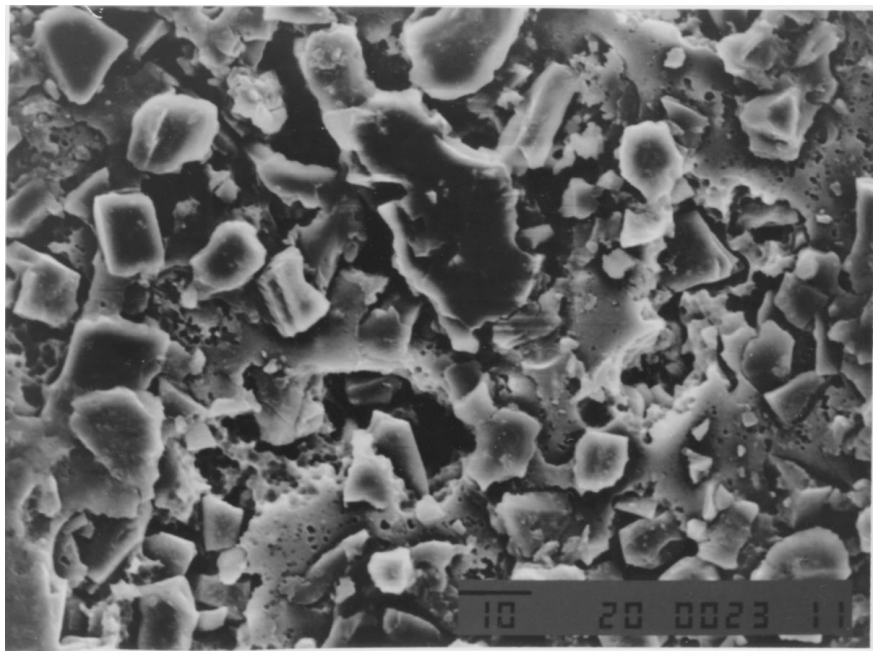

Figure 2 Temper T4 of alloy 6013-20 SiC(P) exposed to 3.5 wt% NaCl at a velocity of 2 m/s at 100°C (×100). Dissolution of oxide and severe attack at SiC/Al matrix is observed.

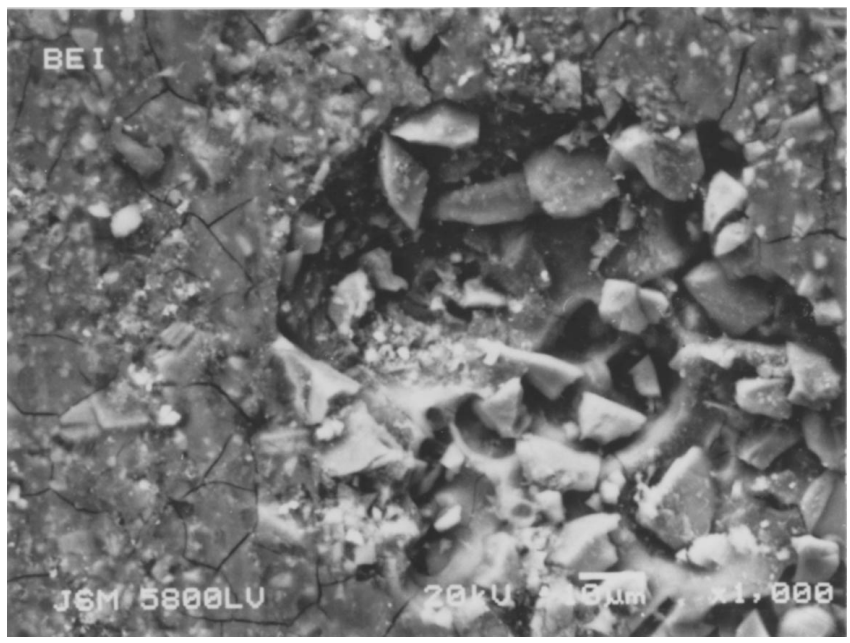

Figure 3 Pitting and intergranular attack observed on the surface of Al 6013-20 SiC(T4) after exposure in 3.5 wt% NaCl.

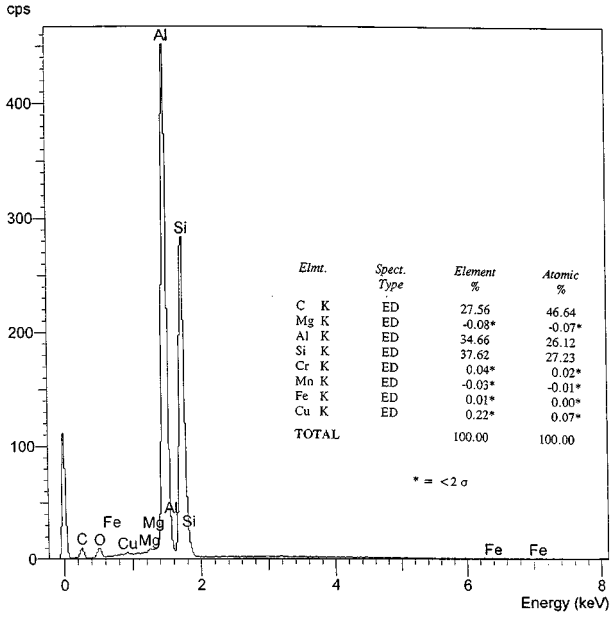

Figure 4 EDS spectrum of temper T4 of alloy 6013-20 SiC(P).

Based on $\Delta E = E_p - E_{corr}$, alloy 6013-20 SiC(P) in temper T4 shows the highest resistance to pitting. In several instances pitting is associated with intergranular attack (Fig. 3). Intergranular attack is not expected in oxygenated chloride solution, unless pits or crevices are presents. In view of the pits present on the surface of Al 6013-20 SiC, intergranular attack is to be expected. The pits are hidden by the precipitation of a gelatinous film of $Al(OH)_3$ which surrounds the pit in the form of chimneys. EDS analysis of the outside surface of the chimneys showed the presence of a soluble complexes of the type $AlCl_x$, Mg and silicon. The pitting behaviour was strongly influenced by heat treatment. Aging alloy 6013-20 SiC(P) at room temperature, after solution treatment at 525°C for 30 minutes (T4) provided higher corrosion resistance than annealing at 350°C for 3 hours and furnace cooling (O-temper), [7] which indicates that microstructural changes predominantly influenced the nucleation and growth of pits.

The microstructure of Al 6013-20 SiC(P)-T4 showed a more homogeneous distribution and lesser clustration of SiC particles. An EDS analysis at 62 eV showed predominantly the presence of Al (34.6%), Si (37.62%) with small amounts of Cu (0.22%) and trace quantities of Fe (Fig. 4).

An abundance of copper intermetallic mainly $CuAl_2$ and secondary phase particles of Mg, Fe and Cu was observed at SiC/Al 6013 interface in temper T4. The amount of copper at the interface between Aluminium matrix and SiC particles was higher than in the matrix (e.g. 0.64% vs 0.34%). The concentration of copper, however, differed from one interface to another. Copper was present in a larger concentration (1.41%) at the SiC/A16013 interface of temper O as shown by EDS analysis (Fig. 5). The presence of varying amounts of copper has been observed in the pit cavities. Pit cavities in T4 temper contain 0.38% Cu with SiC particles. Higher amount of copper (3.5 wt%), Fe (1.77%), Mg (1.71%) with some chloride (0.32%) has been detected

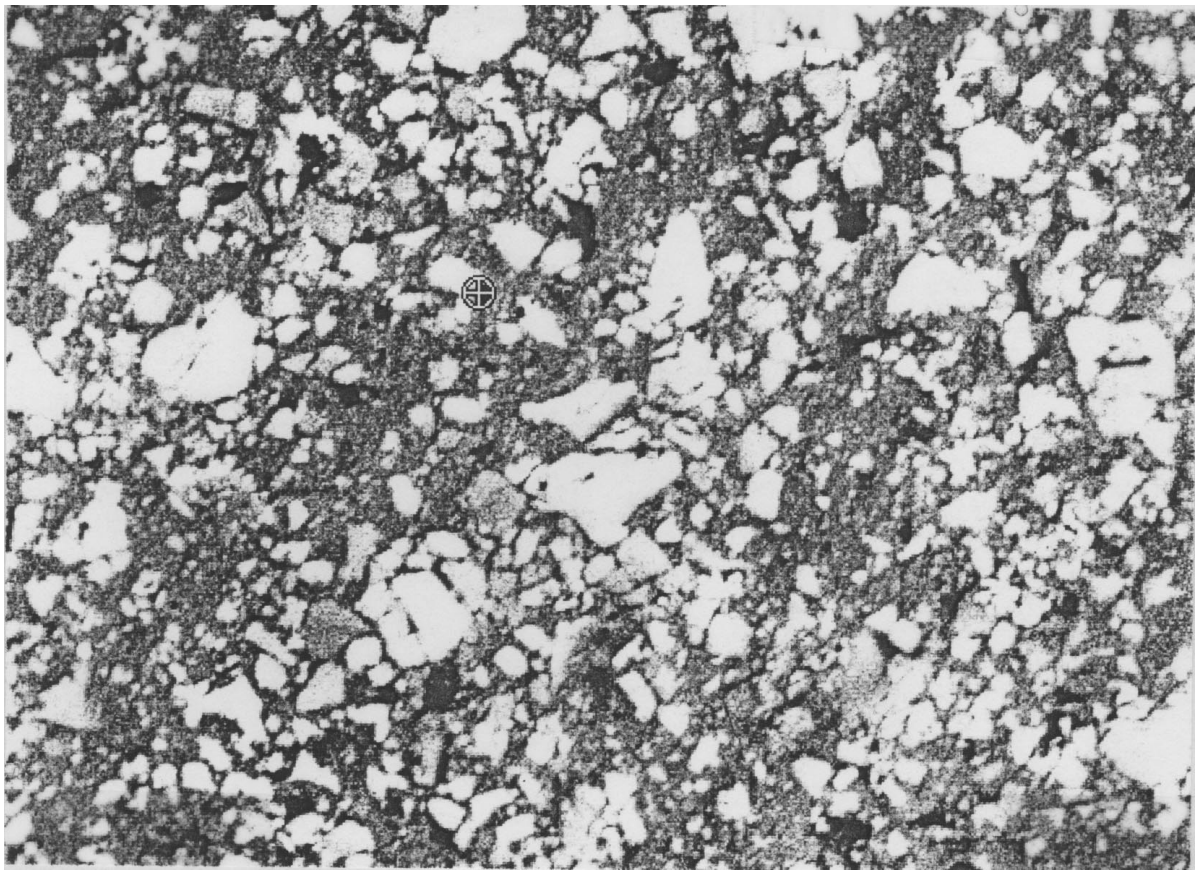

Figure 5 SEM micrograph of O temper of alloy 6013-20 SiC(P). The SiC/Al matrix interface shown by the cursor mark reveals the presence of copper intermetallics.

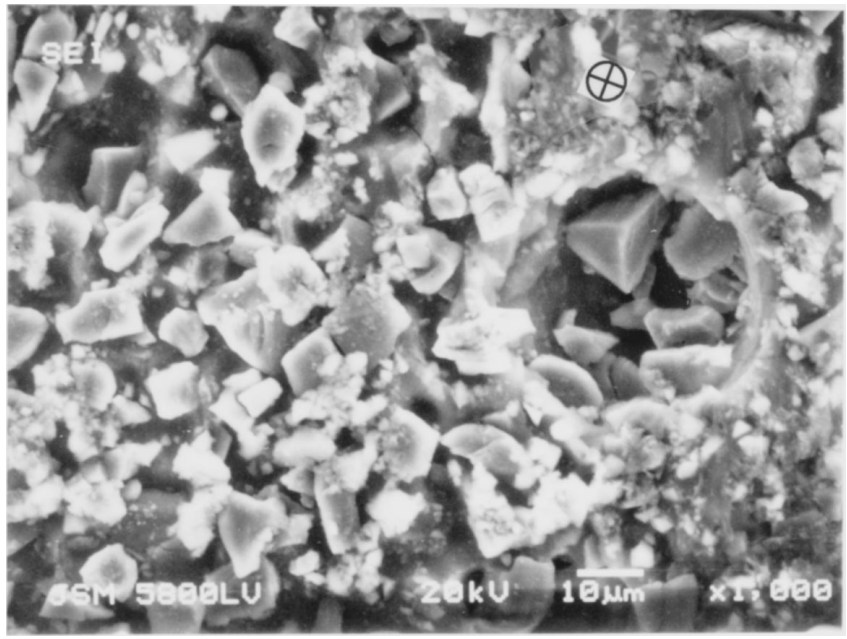

Figure 6 A location of SiC/Al matrix interface shows a high concentration of copper (3.5%), Fe (1.77%), Mg (1.71%) and some Cl (0.32%).

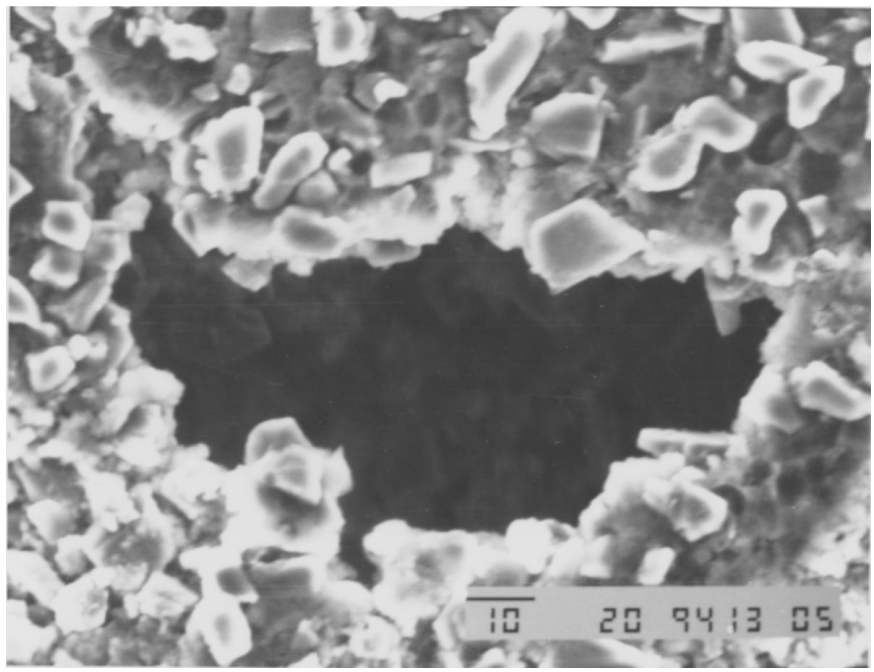

Figure 7 SEM photomicrograph of Al 6013-20 SiC-F showing pitting and carbide particles around the pit (×1500).

by EDS studies on tempers exposed to 3.5 wt% NaCl at velocities varying from 1 m s^{-1} to 3 m s^{-1} (Fig. 6). Pits initiated at the SiC/Al 6013 interface, which is also the preferred site for distribution of intermetallic and secondary phase particles. One pit at a magnification of 1500× is shown in Fig. 7. Corroded region at the interface shows the presence of larger amounts of copper compared to the surface away from the interface as shown by a numerous observations [11]. The presence of $AlCl_3$ in the oxide film has been indicated by EDS studies. The presence of this complex fosters the breakdown of the hydroxide films of boehmite and bayrite (α-AlOOH). Mudcracking (hydroxide breakdown) is shown in Fig. 8. Pits are covered by a gelatinous film of $Al(OH)_3$ in the form of corrosion chimneys (Fig. 9). The formation of Mg_2Si intermetallic at SiC/Al interface causes depletion of Mg and intergranular attack, which is observed in combination with pitting.

When the composite is cooled from elevated temperature processing misfits strains occur due to differential thermal contraction at SiC/A16013 interface [12] which are sufficient to generate dislocations. A TEM micrograph shows generations of dislocations at the interface (Fig. 10) of T4 temper of the alloy. This contributes to the greater reactivity of SiC/Al 60133 interfaces. In the light of the extensive microanalytical experimental work conducted, a strong evidence exists for the following,

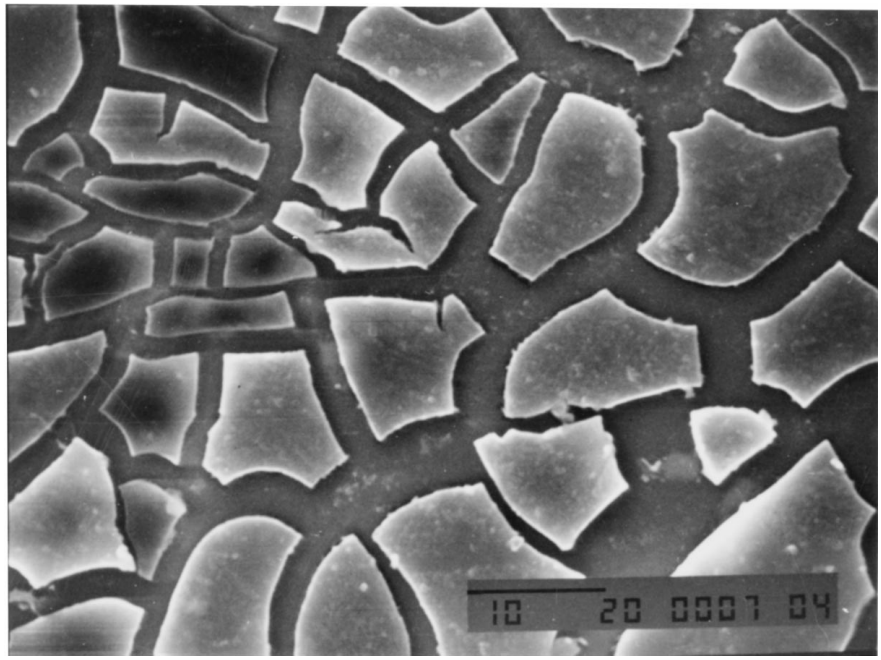

Figure 8 Alloy 6013 (unreinforced) in T4 temper showing clearly the breakdown of oxide layer at the corroded and uncorroded interface.

Figure 9 Pitting accompanied by corrosion chimney formation is observed clearly in O temper of the alloy. The alloy was exposed to 3.5 wt% NaCl at 100°C at a velocity of 1 m/s. Analysis of external surface showed aluminum hydroxide with some chloride, magnesium and silicon (shown by cursor mark).

1. Al 6013/SiC interface shows an increased surface reactivity compared to wrought alloy. This is supported by initiation of pits predominantly at the SiC/A16013 interface.

2. Al 6013/SiC interface is the preferred locations for the intermetallics, mainly of copper and others containing Mg, Fe, and Cu as shown by EDS investigations on the three tempers of the alloy. Higher concentration of copper within the pits and the adjoining surface are caused by copper plating at higher velocities which is in agreement with the work of Mclntyre [13]. The presence of copper at the edge of SiC particles may be attributed to precipitation of these particles during high temperature anneal. Narrow crevices between the agglomerates of SiC particles and matrix showed presence of magnesium and copper. Such sites would be subjected to crevice corrosion.

3. SiC particles do not provide preferred sites for pit initiation. No evidence of corrosion was observed on SiC particles.

4. Because of misfit strains at Al/SiC surface due to thermal contraction, dislocations are generated, which may make interface more reactive and a preferred site for localised corrosion.

5. Chloride is absorbed in the oxide film as shown by the presence of $AlCl_3$ by X-ray diffraction. The adsorption of chloride leads to the breakdown of the protective oxide film. The SiC/Al 6013 interface provides

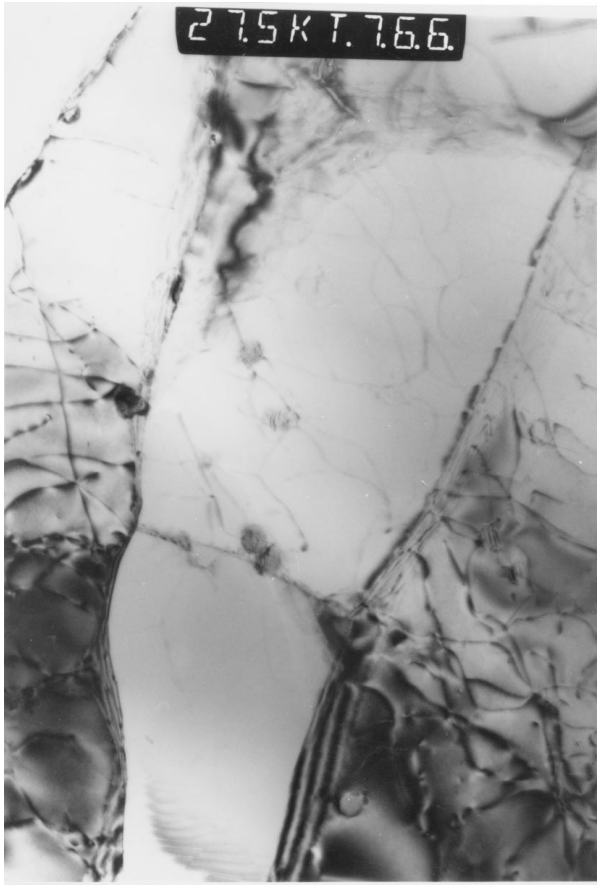

Figure 10 TEM micrograph of Al 6013/SiC interface showing dislocation generations.

preferred sites for breakdown of the protective bayerite and boehmite film. The evidence of breakdown is shown in Fig. 8.

6. The SiC/Al 6013 matrix interface shows the presence of oxide debris due to its breakdown (Fig. 2).

7. Dislocations generations at SiC/Al 6013 contributes to reactivity increases (Fig. 10).

The above observations established that Al 6013/SiC interface is the preferred site for nucleation of pits EDS studies have been successfully used to interpret the pitting process in Al 6013-20 SiC alloy. X-ray diffraction, and ESCA studies were of a limited use only. Earlier work has shown that for alloy Al 5456 pits initiate at the intermetallic phases containing Mg, Cr, Mn, Al and Fe impurities [10]. In SiC reinforced Al 5456, these phases are smaller and more numerous for the same temper. This work in concert with Al 6013-20 SiC provides substantial evidence linking pitting to microstructural changes in aluminum alloy resulting from addition of SiC or heat treatment.

3. Summary and conclusions

Pitting studies on a variety of SiC reinforced and unreinforced aluminum alloys indicate the pitting resistance of SiC reinforced composite materials is dependent upon the alloy type and conditions of fabrication. Initiation of pit at secondary phases on Al 6061 and Al 5456 has been shown in previous work [14]. Investigations conducted on the tempers O, F and T4 of Al 6013 suggest that SiC particles act as a nucleus for secondary phase precipitation which results in a corresponding increased distribution of secondary phase alloy precipitates. SiC/Al 6013 interfaces is the preferred site for breakdown of protective film of α-AlOOH and α-$Al(OH)_3$. Increased dislocation generation at the SiC/Al 6013 interface contributes to increased surface activity. The exact mechanism by which these particles lead to the initiation of a pit is a subject of further investigation.

Acknowledgements

The authors acknowledge the financial support provided by King Abdul Aziz City for Science and Technology and valuable help given by Mr. Saleh and Mr. Reaz is appreciated.

References

1. S. J. CLESIAK, Alcoa, Alloy 6013, Green Letter No. 225, 1987.
2. D. SKLUZAK and Y. TAJIMA. Alcoa, Report No. 90059, 1988.
3. R. C. PACIEJ and V. S. AGARWALA, Naval Aircraft Development Centre, Report NADA 87029-60, 1981.
4. A. H. McINTYRE, S. GOLLEDGE and R. CONRAD, Naval Surface Warfare Centre, Report NSNC, TR, 1987-P 87-326.
5. Z. AHMAD and B. J. ALEEM, *Corrosion* **52**(11) (1996).
6. A. L. GEIGER and J. A. WALKER, *JOM* **43**(8) (1991) 815.
7. P. P. TRZASKOMA, E. McCAFFERTY and C. R. ROWE, *J. Electrochem Soc.* **130** (1983) 1804.
8. E. McCAFFERTY, P. P. TRZASKOMA and P. M. NATISHAN, "Advances in Localized Corrosion" (NACE, Houston, U.S.A) (1990) p. 181.
9. Z. AHMAD, KACST, Dhahran, KSA, KACST Project # AR-14-65. Progress Report No. 2, 1996.
10. A.S.T.M, Annual Book of Standards, Recommended practice, G-61, Vol. 8-03, 1992.
11. Z. AHMAD and A. ALEEM, KACST, Dhahran, KSA, KACST project # AR-14-65, Progress Report No. 5, 1996.
12. M. VOGELSANG, R. J. ARESENAULT and R. M. FISHER, Metallurgical Transactions, **17A** (1986) 376.
13. J. C. M. MCYNTRE, R. K. CONRAD and S. L. GOLLEDGE, *Corrosion* **46** (1990) 902.
14. P. P. TRZASKOMA, *Corrosion* **6**(403) (1990).

Received 30 July 1998
and accepted 15 June 1999